

TWO-ELEMENT OPTICAL ARRAY RECEIVER CONCEPT DEMONSTRATION

¹Victor Vilnrotter, Chi-Wung Lau, Kenneth Andrews, Meera Srinivasan

Jet Propulsion Laboratory, California Institute of Technology
4800 Oak Grove Drive, Pasadena, CA 91109-8009

ABSTRACT

The conceptual design, theoretical performance, and experimental verification of a two-telescope optical array receiver currently under development at the Jet Propulsion Laboratory, is described in this paper. A brief summary of optical communications theory for array reception of pulsed laser signals is developed, and the impact of coding discussed. The development of the optical detection, array processing, and data-acquisition assemblies required for experimental demonstration is described, and preliminary results obtained in a field environment are presented and evaluated.

Keywords: Optical array receiver, communication through turbulence

I. INTRODUCTION

The goal of deep-space optical communications is to relay information from a distant probe to earth in an efficient, cost-effective manner. This goal can be accomplished effectively through the use of optical rather than RF wavelengths. Due to cost and complexity considerations, the most practical approach at optical wavelengths is to employ a ground-based receiver, designed to mitigate the effects of atmospheric turbulence for best performance. A novel approach for ground-based optical communications is the concept of synthesizing a large optical aperture by means of an array of smaller telescopes, each containing a properly designed focal-plane array to reduce losses due to turbulence. Based on theoretical considerations and preliminary experimental results to date, the optical array receiver approach appears to be a viable and robust alternative to single large-aperture optical receivers.

The objective of this research effort is to demonstrate the concept of a ground-based optical array receiver in a relevant field environment, enabling future high data-rate optical communications from space through the application of telescope and photodetector array algorithms and signal processing techniques. The theoretical foundations of optical array reception through atmospheric turbulence has been developed and documented in [1, 2, 3]. These theoretical results have now been extended to include a preliminary field demonstration of key optical components and array receiver concepts, through a combination of analysis, field data-acquisition and offline signal processing. The ultimate goal is to demonstrate a realistic optical array receiver in a relevant field environment, with high-rate pulse-position modulated (PPM) optical signals received, detected, and decoded in real-time.

II. DATA RATE AND PHOTON EFFICIENCY

An accepted metric for assessing communications system performance is the rate at which information can be transferred between the transmitter and the optical receiver. The rate of digital communications is measured in terms of the number of bits of information transferred to the receiver each second, denoted by the symbol R , in units of

¹ The research described in this publication was carried out by the Jet Propulsion Laboratory, California Institute of Technology, under a contract with the National Aeronautics and Space Administration.

bits/second. In addition to data rate, another important aspect of communications performance is fidelity, that is, the accuracy with which the transmitted information can be recovered at the receiver despite space loss, background radiation, noise in the receiver electronics, and distortions introduced by the physical channel. The fidelity of the received data can be measured in terms of “error probability”, that is, the probability that the received data bits, or symbols, are interpreted correctly at the receiver. With an optical array receiver, the signal photons detected at each telescope must first be combined with the correct timing, then synchronized with the receiver clock and demodulated by the optical receiver. We perceive that higher the data-rates imply better performance, provided that a certain predetermined level of fidelity, specified in terms of error probability, can be maintained.

The rate of information transfer in any optical communications system, R , can be conveniently separated into the product of two distinct terms: one that takes into account the physical attributes of the channel, and another that specifies modulation and coding efficiency. Denoting the average number of photons detected in a T second interval by K_s , we can define the “signal photon rate” at the receiver by $n_s = K_s / T$ with units of photons/second. Then the “photon information efficiency” ρ , with units of bits/photon, is the rate of information transfer, and can be expressed as

$$R = \rho n_s \text{ bits/second} \quad (1)$$

The term that describes physical effects, n_s , is directly related to the output power of the laser transmitter aboard the spacecraft; the gain of the transmitting antenna; pointing accuracy; space-loss and other losses due to atmospheric effects; and the size and transmittance of the receiving optics. All of these factors contribute to the total signal power delivered to the optical array receiver. It is intuitively clear that higher signal power leads to improved communications: however, different modulation and coding schemes may operate at significantly different photon information efficiencies, which also affects the communications rate. Therefore, to achieve high rates of information transfer between the transmitter and the receiver, modulation and coding schemes capable of high information efficiencies are required.

III. MODULATION AND DETECTION FOR THE OPTICAL ARRAY RECEIVER

The information rate ρ achievable by an optical array receiver depends on the modulation format employed, and on the coding applied to the modulated optical symbols. The advantages of optical Pulse Position Modulation (PPM) have been described in [4], and shown to have highly desirable properties when operating at practically realizable information efficiencies, such as: low average power requirements; resistance to background radiation; and ease of implementation with currently available laser modulation techniques. Other modulation formats suitable for optical arrays include “multi-pulse PPM” as described in [5], “on-off keying” (OOK) and “optical frequency-shift keying” (OFSK), however here we focus on optical PPM, which is the modulation format receiving the greatest attention for deep-space communications.

Optical PPM is well suited to existing laser modulation techniques (such as Q-switching, mode-locking and cavity-dumping), requires low average power, attains high information efficiencies, and is resistant to background radiation. Theoretically, this modulation format consists of a fixed number of symbols, M , of equal duration, T seconds. Assuming that M is a power of two, $M = 2^L$, and recalling that the number of bits of information contained in a PPM symbol is $\log_2 M$, we can view the mapping from information-bits to PPM symbols as a one-to-one assignment of symbols to each of L consecutive information bits.

A pictorial description of received PPM symbols is illustrated in Fig.1. The sample is the smallest time interval over which integration and sampling can be carried out, and is determined by digital hardware limits and computational constraints. In order to establish slot-synchronization a minimum of two samples may be needed [4], but there is no conceptual upper limit to the number of samples per slot provided that number is even. PPM modulation consists of mapping each sequence of L data-bits into one of $M = 2^L$ slot-locations according to a predetermined look-up table,

and firing the laser so as to place the optical pulse in the correct slot relative to the previous pulse. With no loss in generality, we include a dead-time of N slots following the M signal slots, for a total of $M+N$ "frame" slots: this generalized model applies to Q-switched lasers at the spacecraft transmitter, which typically require a dead-time after firing each pulse to repopulate the lasing medium after depletion: however, our model applies to amplified solid-state transmitters as well, corresponding to the case $N = 0$.

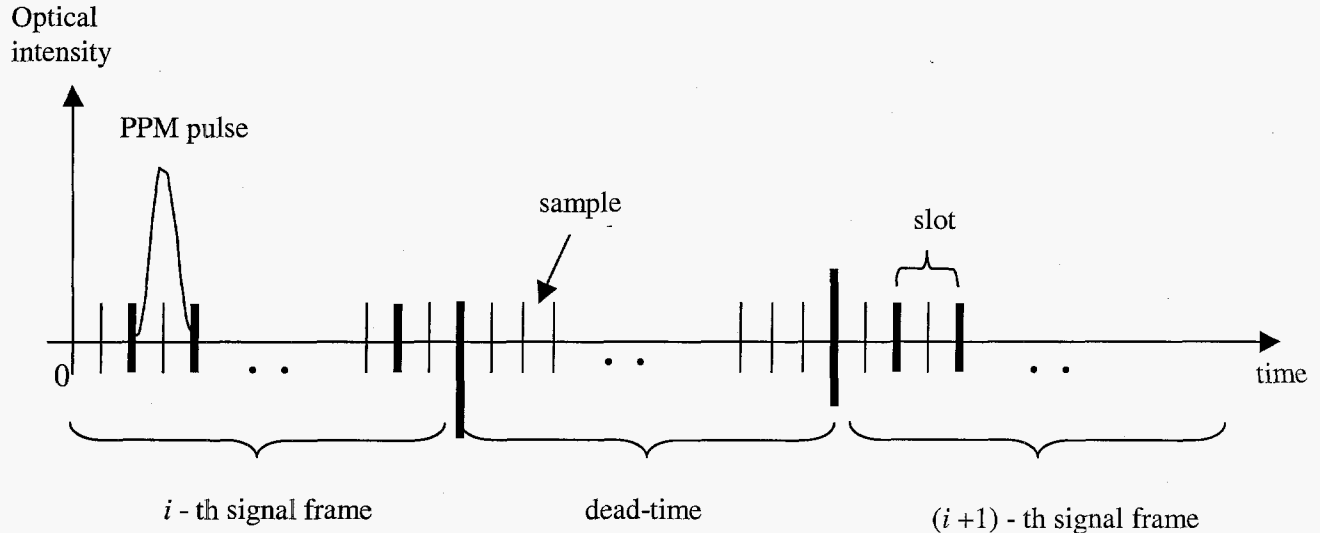


Figure 1. Pulse Position Modulation format illustrating samples, slots and possible dead-time.

The number of photons in a coherent-state optical field generated by lasers is Poisson-distributed [4], therefore we shall adopt this model to describe the statistics of the observable processed by the receiver. We further assume that the optical fields have been detected with a high quantum efficiency photon-counting detector. The probability of detecting k photons, $P(k)$, $k \geq 0$, is given by the expression

$$P(k) = \frac{K_s^k}{k!} e^{-K_s} \quad (2)$$

At the array receiver, the sum of the detected photons in each slot from all array elements are counted and the slot with the greatest photon-count declared to be the signal-slot, hence the PPM symbol corresponding to signal energy in that slot is selected.

An accepted detection strategy for minimizing the average probability of symbol error when the a priori probabilities are known is the *maximum a-posterior*, or MAP, detection strategy. If there is no appreciable background radiation, an erasure over any of the signal-slots occurs with probability e^{-K_s} when the detection process is governed by Poisson statistics. If no counts whatsoever are observed in any of the slots from any of the array detectors, then the MAP strategy makes use of the a priori information: if the a priori symbol probabilities are equal, a random selection strategy is employed, increasing the detection probability slightly over assigning the erasure to an "error" by guessing correctly one out of M times on the average. Therefore, the probability of detecting the transmitted PPM symbol correctly is one if any number of photons greater than zero are observed in the signal-slot, and $1/M$ if no photons whatsoever are observed:

$$\begin{aligned} P_M(C) &= P(C | k \geq 1) \Pr(k \geq 1) + P(C | k = 0) \Pr(k = 0) \\ &= 1 \times \left[1 - e^{-K_s} \right] + \frac{1}{M} \times e^{-K_s} \\ &= 1 - e^{-K_s} \left[1 - \frac{1}{M} \right] \\ &= 1 - \frac{M-1}{M} e^{-K_s} \end{aligned} \quad (3)$$

The probability of symbol error is related to this quantity as:

$$P_M(SE) = 1 - P_M(C) = \frac{M-1}{M} e^{-K_s} \quad (4)$$

Once the PPM symbol is detected, it is mapped to a string of L bits via the inverse of the encoding mapping. If the PPM symbol has been detected correctly, then every bit of the resulting L -bit sequence will be correct. However, in the event of a symbol error, only half of the bits will be incorrect, on the average.

As described above, an alternate indicator of communications system performance is the information efficiency, defined as $\rho = \log_2 M / K_s$ bits/photon for orthogonal signals. When communicating with T -second M -ary PPM symbols, the data-rate is

$$R = \rho n_s = \frac{\log_2 M}{K_s} \frac{K_s}{T} = \frac{\log_2 M}{T} \text{ bits/second} \quad (5)$$

at an average rate of $n_s = K_s / T$ photons/second observed by the array.

It is useful to express the bit error probability in terms of the information efficiency, as this provides a direct method to determine system efficiency when operating at a prescribed error probability. This can be accomplished analytically when there is no background radiation, by writing K_s in terms of ρ and substituting into equation (5):

$$\begin{aligned} P(E) &= \frac{1}{2} e^{-\log_2 M / \rho} \\ &= \frac{1}{2} M^{-\log_2 e / \rho} \\ &= \frac{1}{2} M^{-1.44 / \rho} \end{aligned} \quad (6)$$

The result shows that operating at high values of ρ tends to result in high error probabilities, at any value of M . By generating plots of the error probability as a function of ρ , the information efficiency of the array can be determined at any error probability.

The presence of background radiation does not alter the detection algorithm significantly, which now selects the slot containing the greatest total number of signal plus background photons. However, with non-zero average energy in each slot due to background, there is a possibility of multiple maximal photon-counts, in which case the MAP decoding strategy relies on a random choice among those slots with the greatest count. Letting r denote the number of maximal counts, and taking into account all possible ways that r equalities can occur among M slots, the probability of correctly detecting the laser pulse in the presence of background radiation generating an average of N_b background photons per slot, can be expressed as

$$\begin{aligned} P_M(C) &= \left\{ \sum_{r=0}^{M-1} \binom{M-1}{r} \sum_{k=1}^{\infty} \frac{(K_s + K_b)^k}{k!} e^{-(K_s + K_b)} \left[\frac{(K_b)^k}{k!} e^{-K_b} \right]^r \left[\sum_{j=0}^{k-1} \frac{(K_b)^j}{j!} e^{-K_b} \right]^{M-1-r} \right\} \\ &+ M^{-1} e^{-(K_s + MK_b)} \end{aligned} \quad (7)$$

with corresponding error probability $P_M(E) = 1 - P_M(C)$.

III. OPTICAL ARRAY RECEIVER MODEL AND PERFORMANCE

In the following section we assume that the optical bandwidth of each telescope front-end is much greater than its electrical bandwidth, so that a “multimode” assumption can be applied to both the signal and background fields (this assumption is generally true even with extremely narrow optical filters of approximately 1 angstrom bandwidth and high-rate digital sampling. It has been shown that multimode Gaussian fields with suitably small average modal noise count generate approximately Poisson distributed random point processes at the output of an ideal “photon-counting” detector [4]. This model is valid for communications systems operating at gigabit rates, and justifies the use of the relatively simple Poisson model which, in turn, often leads to mathematically tractable solutions.

Consider an array of optical detectors consisting of a total number of $K \times L$ detector elements, representing K detector elements per telescope (denoted as the “focal-plane array”, or FPA) and L telescopes comprising the array receiver, as in [1,3]. Assuming a “frozen atmosphere” model, the sample function density of an array of count observables from a particular focal-plane detector element of a given telescope can be written as $p[N_{mn}(t) | \lambda_{mn}(t); 0 \leq t < T]$. The joint conditional sample function density over the entire array can be expressed in terms of the KL dimensional vector $\mathbf{N}(t)$ as

$$p[\mathbf{N}(t) | \lambda(t); 0 \leq t \leq T] = \prod_{m=1}^K \prod_{n=1}^L p[N_{mn}(t) | \lambda_{mn}(t); 0 \leq t < T] \quad (8)$$

where $\mathbf{N}(t) \equiv (N_{11}(t), N_{12}(t), \dots, N_{KL}(t))$. This detection model applies whenever the desired information is contained in the intensity distribution, but only the array of count accumulator functions can be observed. For the case of PPM signals, a laser pulse of duration τ seconds is transmitted in one of M consecutive time-slots, resulting in a PPM symbol of duration $T = \tau M$ seconds. As shown in [6], the log-likelihood function can be expressed as:

$$\begin{aligned} \Lambda_i(T) &= \sum_{m=1}^K \sum_{n=1}^L \left\{ \sum_{w_{j,mn} \in ((i-1)\tau, i\tau]} \ln \left(1 + \frac{\lambda_{s,mn}(w_{j,mn})}{\lambda_b} \right) \right\} \\ &= \sum_{m=1}^K \sum_{n=1}^L \ln \left(1 + \frac{\lambda_{s,mn}}{\lambda_b} \right) N_{mn}^{(i)} \end{aligned} \quad (9)$$

where $N_{mn}^{(i)}$ is the total number of photons occurring over the m -th detector element in the focal-plane of the n -th telescope during the i -th time-slot. Note that with constant signal intensities the actual arrival-times of photons within each slot do not contribute to the decision, hence only the total number of detected photons, $N_{mn}^{(i)}$, is used. Given that we know the optical intensity over each detector element at each instant, the i -th log-likelihood function consists of the sum of a logarithmic function of the ratio of signal and background intensities from all detector elements over the i -th pulse-interval, multiplied by the total number of detected photons: the optimum detection strategy is to select the symbol corresponding to the greatest log-likelihood function as defined in (11).

The probability of a correct decision is the probability that the log-likelihood function associated with the transmitted symbol exceeds all other log-likelihood functions. Thus, when the q -th symbol is sent, a correct decision is made if $\Lambda_q(T) > \Lambda_i(T)$ for all $i \neq q$. Denoting the logarithmic functions, or “weights”, in (11) by $u_{mn}^{(i)}$, the log-likelihood function (11) can be rewritten as:

$$\Lambda_i(T) = \sum_{m=1}^K \sum_{n=1}^L u_{m,n}^{(i)} N_{mn} \quad (10)$$

In this form, we can see that the log likelihood function is composed of sums of a random number of weights from each detector element: for example, the m -th detector element in the n -th telescope contributes an integer number of its own weight to the sum. Note that detectors containing much more background than signal do not contribute significantly to the error probability, since the outputs of these detector elements are multiplied by weights that are close to zero. This observation suggests the following suboptimum decoder concept resulting in simplified processing: list the detector elements from all telescopes simultaneously, starting with the detector containing the most signal energy, followed by every other detector in order of decreasing signal intensity. In effect, the logarithmic weights are partitioned into two classes: "large" weights are assigned the value one, while "small" weights are assigned the value "zero". It was shown previously [6] that this simple partitioning achieves near-optimum performance in low to moderate background environments, but with reduced decoder complexity.

The probability of a correct decision for an array that employs those detectors containing much more signal than noise, as described in [6,] can be obtained by assuming constant signal and background intensities over each time-slot, yielding the conditional Poisson densities

$$p_q(k | H_q) = \frac{(\lambda_s \tau + \lambda_b \tau)^k}{k!} e^{-(\lambda_s \tau + \lambda_b \tau)} \quad \text{and} \quad p_i(k | H_q) = \frac{(\lambda_b \tau)^k}{k!} e^{-\lambda_b \tau} \quad (11)$$

$$P_M(C) = \left\{ \sum_{r=0}^{M-1} \binom{M-1}{r} \left(\frac{1}{r+1} \right) \sum_{k=1}^{\infty} \frac{(\lambda_s \tau + \lambda_b \tau)^k}{k!} e^{-(\lambda_s \tau + \lambda_b \tau)} \left[\frac{(\lambda_b \tau)^k}{k!} e^{-\lambda_b \tau} \right]^r \left[\sum_{j=0}^{k-1} \frac{(\lambda_b \tau)^j}{j!} e^{-\lambda_b \tau} \right]^{M-1-r} \right\} + M^{-1} e^{-(\lambda_s + M\lambda_b)\tau} \quad (12)$$

The probability of symbol error then follows as $P_M(E) = 1 - P_M(C)$. This adaptive array receiver concept estimates the signal and background on a timescale short compared to the turbulent intensity variations in the focal-plane.

IV. CODING TO IMPROVE ARRAY PERFORMANCE WITH PPM SIGNALS

Following photon-counting detection at each telescope, the signals are aligned in time, then combined, and detected using the maximum likelihood strategy described above. There are many options for encoding the PPM symbols before transmission to reduce errors or increase the throughput at a given bit error rate (BER), but here we consider only the well-known Reed-Solomon codes that can be applied to PPM signaling following maximum likelihood symbol detection. First we consider the case of negligible background radiation, then extend these results to the more general case.

It has been shown that Reed-Solomon coded optical PPM is a very effective coding scheme that achieves high information rates over the optical erasure channel [7], with substantial coding gains for optical channels encountered in practice. Reed-Solomon codes are a non-binary subclass of BCH codes that achieve the largest possible code minimum distance for any linear code [8]. Codewords consist of strings of N PPM symbols, selected out of the M^N possible sequences. If binary data-sequences of length L are mapped into PPM symbols as before, then the number of PPM symbols required to represent every possible binary sequence is $M = 2^L$. Using strings of length N to generate the codewords, Reed-Solomon codes have the following structure: codewords are formed as strings of length

$N = 2^L - 1 = M - 1$; of the N symbols, $k < N$ can be considered as data-symbols, where

$k = 2^L - 1 - 2t = N - 2t$; the minimum distance is given by $d_{\min} = N - k + 1 = M - k$. The code corrects any combination of t or fewer symbol errors, $t = \frac{1}{2}(d_{\min} - 1) = \frac{1}{2}(n - k)$ hence requires no more than $2t$ parity-check

symbols. Since the total number of data-symbols is M^k , it follows that each codeword represents $\log_2 M^k = k \log_2 M = k \log_2 2^L = kL$ bits of information. If each of the N PPM symbols contains a received laser pulse in one of M slots of average photon-energy K_s photons, the information-rate for Reed-Solomon codewords is given by

$$\rho = \frac{\log_2 M^k}{NK_s} = \frac{kL}{NK_s} = r \frac{L}{K_s} \text{ bits/photon} \quad (13)$$

where the “code rate” is defined as $r \equiv \frac{k}{N}$.

With hard decision decoding, maximum likelihood symbol decisions are sent to the RS decoder, which corrects all patterns of t or fewer errors. With p denoting the channel error probability, the probability of symbol error can be approximated by the following expression [8]:

$$P_S(E) \cong (2^m - 1)^{-1} \sum_{k=t+1}^N k \binom{N}{k} p^k (1-p)^{N-k} \quad (14)$$

Since Reed-Solomon codes are cyclic, the probability of any particular PPM symbol being in error, given a codeword error, is d_{\min} / N . Taking into account the conversion between PPM symbol and bit error probabilities, the bit error probability can be expressed approximately as

$$P(E) \cong \frac{M/2}{M-1} \left(\frac{d_{\min}}{N} \right) PWE \quad (15)$$

This expression will be used to approximate the Reed-Solomon coded performance of the two-element optical array receiver in the following section.

V. TWO-ELEMENT OPTICAL ARRAY RECEIVER FIELD EXPERIMENTS

The research effort reported in this article extends the theoretical investigations reported in [1, 2, 3] by constructing a two-telescope optical array receiver, capable of collecting and processing pulsed laser data in a relevant field environment. As a first step, this demonstration required the development of a detailed system design that identified the signal processing functions, followed by development and integration of key components. Simultaneously, signal processing algorithms capable of compensating adaptively for differential delay-variations between the telescopes were developed and evaluated. The receiver front-end of each telescope was constructed and tested using custom designed experimental photon-counting detector arrays. In addition, a low-power laser transmitter assembly was constructed for generating weak laser pulses simulating pulse-position modulation. The purpose of these initial experiments was to record sample-streams generated by both telescope front-ends simultaneously, then process the recorded data to demonstrate array compensation capability as well as communications gain.

1. Optical Array Receiver System Concept

A conceptual block diagram of the signal processing functions necessary for arraying direct detected optical signals is shown in Figure 2. Electrical pulses from each $N \times N$ focal-plane detector array are processed in the “FPA Electronics Card” of each telescope to determine the total number of detected photons per sample-time, and to extract local information such as telescope pointing updates and instantaneous estimates of the focal-plane intensity distribution to further reject background photons via adaptive focal-plane processing as described in [6]. Digital samples are then constructed at each telescope to facilitate transfer to a central Array Combiner Assembly, which compensates the sample-streams to remove possible delay variations before combining thus maximizing the signal energy in each signal-slot, and simultaneously minimizing the pulse-widths. After combining the delay-compensated samples, the Array Combiner Assembly transmits a single sample-stream with maximized pulse-energy to the digital receiver, which then proceeds to synchronize the combined digital pulses with the received optical pulses, and continuously adjusts the total

delay to track any residual doppler not accounted for by predicts. The Array Combiner Assembly may also receive a synchronized PPM reference clock from the receiver, along with symbol decisions and other side information useful to the array, and distributes these references to the array telescopes as needed.

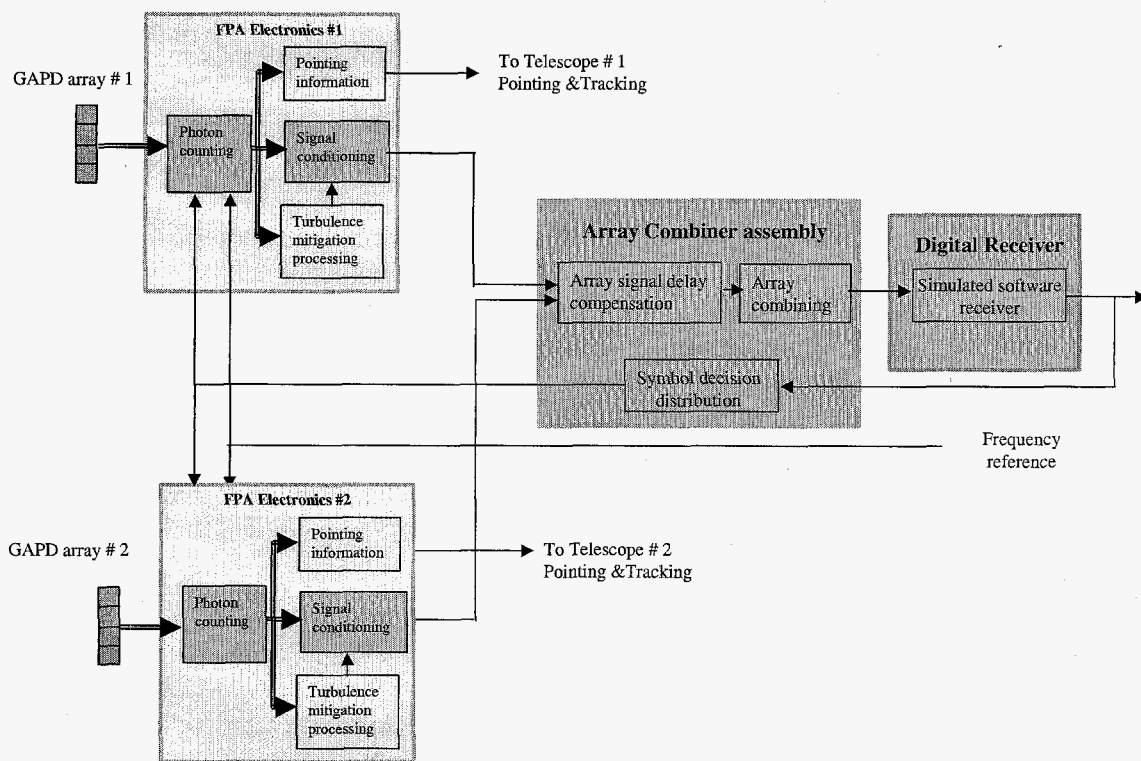


Figure 2. Conceptual block diagram of optical array receiver

2. Two-Element Optical Array Experimental Configuration

After initial testing of the 25" computer-driven telescope in [2], a second 25" telescope was procured from the same manufacturer (JMI, Inc., of Colorado) in 2004. A preliminary low-intensity experimental setup, completed in August 2004 on the JPL mesa antenna test range, was used to receive signal photons from a retro-reflector assembly located approximately 210 feet away. The retro-reflector assembly consisted of a 65 mm diameter corner-cube reflector equipped with a long focal-length lens, operating in an optical double-pass configuration: this arrangement expands the weak retro-reflected laser beam sufficiently to span the distance between the two telescopes. The laser transmitter assembly is consisted of a 5 milliwatt maximum power, 635 nm laser mounted in a fine-pointing bracket, and a pulse generator configured for 1 microsecond pulses repeating at 16 microsecond intervals. The laser is effectively gated "on" by the 1 microsecond pulses, and "off" for the following 15 microseconds, simulating a simple repetitive 16-PPM symbol suitable for initial testing. The gating operation further dilutes the average power of the transmitted signal by a factor of 16, yielding an effective transmitted laser power of $5/16 = 0.3125$ milliwatts leaving the laser, which then enters a $10\times$ microscope objective to further increase the divergence of the captured laser beam, generating a footprint 10 ft in diameter at the retro-reflector assembly. The retro-reflector captures a small fraction of the optical signal and reflects it back towards the two-element telescope array.

3. Photon-counting Detector Array Assemblies

The received optical energy was focused in each telescope and directed to a real-time CCD camera manufactured by SBIG, Inc., to extract position and intensity information prior to data-acquisition. The position information was used to fine-point the telescopes towards the retro-reflected beam. Following spatial acquisition, the CCD camera in each

telescope was replaced by a high sensitivity geiger-mode avalanche photodiode (GAPD) detector array assembly custom-built by aPeak, Inc., shown in Figure 3a. These GAPD detector arrays consist of 4×4 detector elements, where each detector is capable of counting individual detected photons and generating a large (nominally 3 volt) pulse of 50 nanosecond duration in response to a photon detection event, as shown in Figure 3b. During field experiments, numerous signal photons could be detected with the highest pulse intensities, delayed with respect to the driving electrical pulse due to the lagging response of the laser and drive electronics plus the round-trip light-time of approximately 420 nanoseconds, as illustrated in Figure 4c. A few background and “dark-count” photons can also be seen occurring randomly on the oscilloscope screen.

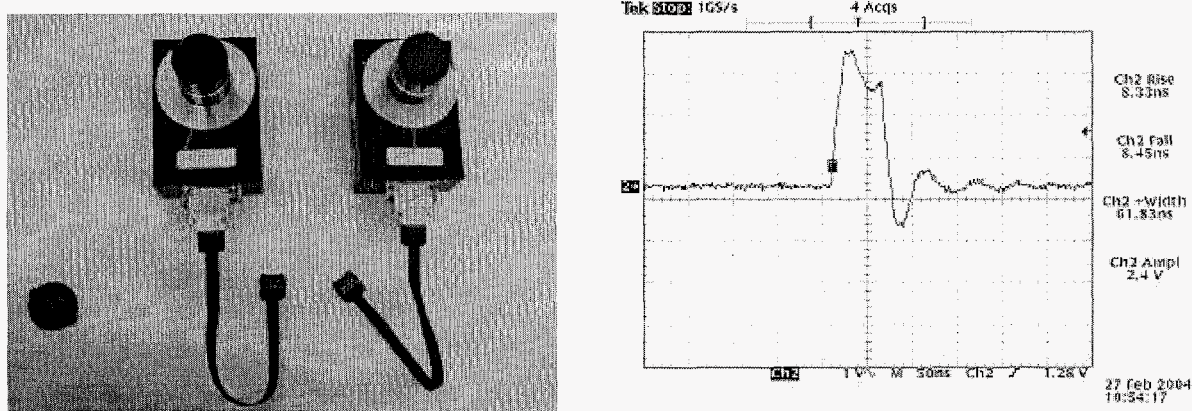


Figure 3 a) Photon-counting detector arrays manufactured by aPeak, Inc. b) Typical response of a detector array element to a single detected photon.

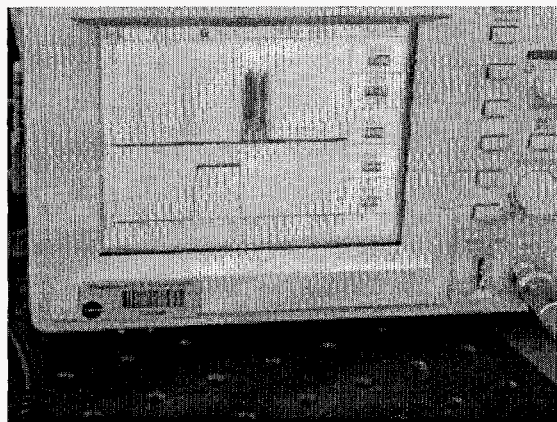


Figure 3 c. Response of an array detector element to pulsed laser signals in the field: lower trace is the electrical signal driving the pulsed laser; upper trace is the detector response showing a cluster of detected photons delayed by propagation and instrument delays (note randomly occurring photon-detection events due to background radiation and detector dark counts)

4. Data Acquisition Assemblies

The streams of electrical pulses generated by each detector array are captured by high-speed logic analyzer assemblies manufactured by GoLogic, and stored as samples of 8 nanosecond binary data, where each “1” represents a detector output voltage that exceeds a preset threshold (nominally 1 volt), while each zero represents lack of an output pulse. Therefore, a nominally 50 nanosecond electrical pulse is typically represented as a sequence of 6 – 7 binary ones, where each sample is of 8 nsec duration. Each logic analyzer captures 4 million samples from every detector of the array, for a total of 64 mega-samples per file. As currently configured, each data file represents approximately 30 milliseconds of data, stored as four hexadecimal numbers: each hex number represents the distribution of ones and zeros in four channels for a given sample, so that four hex numbers are required to represent all sixteen detector array outputs. The two logic analyzers have been configured for synchronous operation, enabling simultaneous data-acquisition from the two

telescopes. However, for efficient data-gathering in the field, it was necessary to use a separate computer for each logic analyzer to record the data.

5. Delay Compensation and Array Combining Algorithms

After each field experiment the data was processed offline using custom algorithms, and the results analyzed to help improve the quality of the data-set during the next experiment. First, the binary outputs from the sixteen channels of each GAPD detector array are summed together. Since the detector output pulses tend to be approximately 50 nanoseconds in duration, the sampled electrical output pulses occur as runs of 6 or 7 “ones”, and the transitions from zero to one are summed to obtain the photon counts. The current processing algorithms do not allow for optimal or near-optimal weighting of the individual detector output channels to account for the effects of particularly noisy detector elements or atmospheric turbulence: in this preliminary version, only the summed output of the entire focal-plane detector array is used. However, the added capability of optimal channel weighting will be incorporated in the next generation of signal processing algorithms.

The summed channel signals are converted to samples and a new data-file created, which serves as input to the adaptive delay-compensation algorithm. This algorithm was developed specifically for PPM signals detected with photon-counting detectors, and is intended to compensate for slowly-varying delay drift to ensure that PPM pulses received from each telescope are properly aligned in time before combining. The adapted delays for the i^{th} telescope (here i is either one or two, since there are only two telescopes) are formed according to an algorithm that resembles the well-known least mean square (LMS) and “constant modulus algorithm” (CMA) often employed to “phase up” conventional radio frequency arrays [1], except that here the delay adaptation is based entirely on the observed photon-counts. Denoting the PPM slot number by n and the delay variable by τ , the delay update algorithm for the i^{th} telescope is of the form:

$$\tau_i(n+1) = \tau_i(n) - \mu \left(\sum_{j \in \text{slot}} y_j(n) - y_0 \right)^2 \left[\sum_{j \in \text{slot} / 2}^{slot-end} s_{ji}(n) y_j(n) - \sum_{j \in \text{slot} - start}^{slot / 2} s_{ji}(n) y_j(n) \right] \quad (22)$$

*

previously
cleaned?

where j is the index of the sample within the n^{th} slot, $s_{ji}(n)$ are the summed photon-counts from the i^{th} telescope over the j^{th} sample of the n^{th} slot, $y_j(n)$ is the summed photon-count output of all telescopes over the j^{th} sample of the n^{th} slot, y_0 is the desired combined average photon-count of perfectly combined PPM sequences (usually determined from predicted or measured received signal power levels), and μ is the stepsize that controls the rate of the algorithm’s convergence and the degree of smoothing. The error signal is seen to be the difference in the correlations of the received photon-count samples and the combined photon-count samples from the first and second halves of each slot. When the cost function approaches zero, the algorithm stops updating and continues to supply time-aligned combined samples to the receiver for further processing. An example of the array output resulting from processing two-telescope array field data, and of the behavior of the cost function as the delay differences were reduced by the algorithm, is shown in Figure 4. Note that the cost function rapidly approaches zero, indicating that the two sample-streams have been effectively aligned after only a few PPM symbols have been processed.

6. Communications Performance of the Optical Array Receiver

Following delay compensation and combining, the software receiver forms sufficient statistics from the received combined samples, which in this case reduce to sums of sample-counts over each PPM slot. The optimum detection algorithm compares the slot-count over each PPM symbol and selects the symbol corresponding to the greatest slot-count [2, 3]. Since in our field experiments the signal pulse always occurred in the first slot, performance can be determined by comparing the symbol-decision made by the receiver with the known pulse location. This processing and

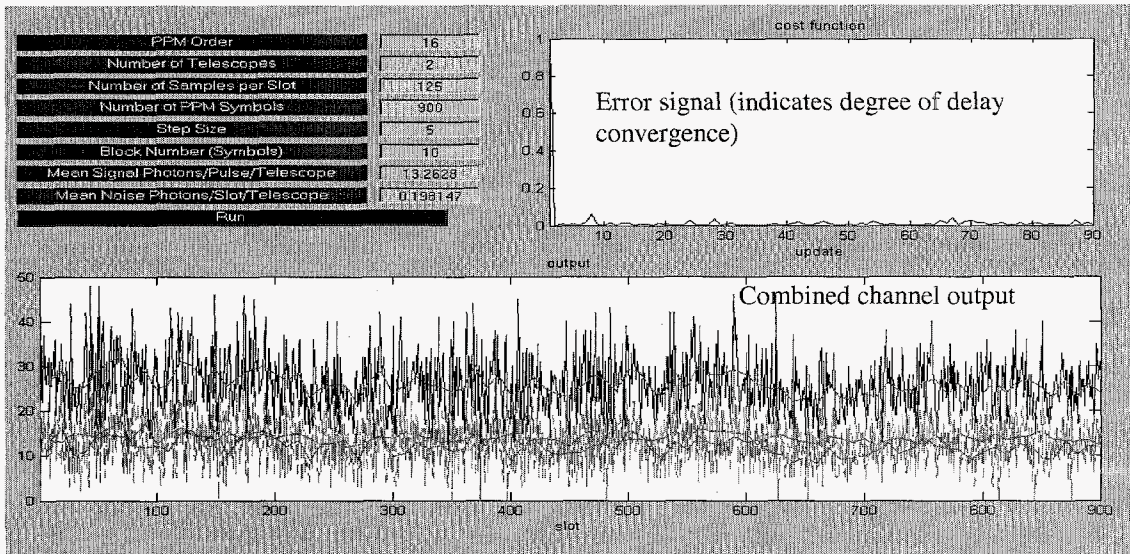


Figure 4. Two-telescope field data processed by the adaptive delay compensation and combining algorithm

error-estimation was carried out on data-sets taken in September, 2004. After telescope alignment, data was taken with various neutral density filters placed in front of the transmitter laser to attenuate the signal in controlled steps.

The results of this initial data set taken in September, 2004, are shown in Figures 5a and 5b, where the symbol error rate (SER) performance of the array, together with the SER of each individual telescope, is shown both as a function of transmitter attenuation (filter density ND) and average photon-count per PPM signal-slot, K_s . In these initial data-sets only a few attenuations were used: the received laser power was weak to begin with, therefore the SER in these data-sets was generally quite high, in the neighborhood of 0.5 to nearly 1. This range, however, represents a reasonable operating region for coded operation, where subsequent decoding of the detected PPM symbols can yield much lower bit error probabilities. Note that in all cases, array performance is significantly better than the performance of the individual telescopes taken separately.

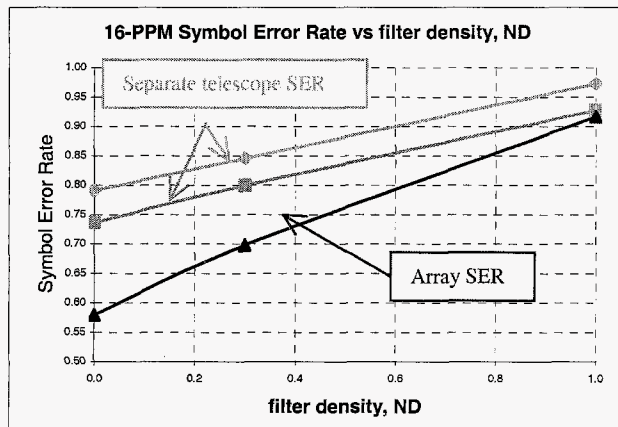


Figure 5a. Symbol error probability of experimentally obtained 16-PPM data, as a function of filter density ND.

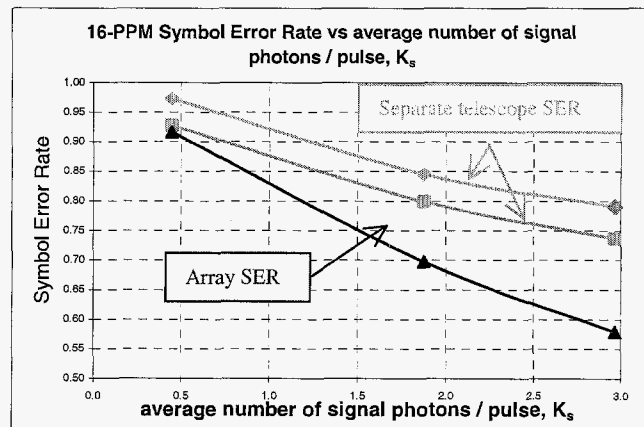


Figure 5b. Symbol error probability of experimentally obtained 16-PPM data, as a function of average signal-pulse photon count, K_s .

The experimental setup was modified in December 2004 to enable the reception of stronger laser signals directly from a pulsed laser located approximately 140 feet from the array telescopes, in order to evaluate array performance at much lower error probabilities. This upgraded experimental setup also anticipates a more realistic configuration where the laser transmitter will be placed on the mesa transmitter facility located approximately 1 km from the array. Figure 6 shows the location of the array telescopes at the entrance of building 256A on the mesa, and the laser transmitter assembly located at the edge of the mesa: the mesa transmitter facility where the laser will eventually be located for testing under more realistic atmospheric turbulence conditions can be seen on the other side of the valley.

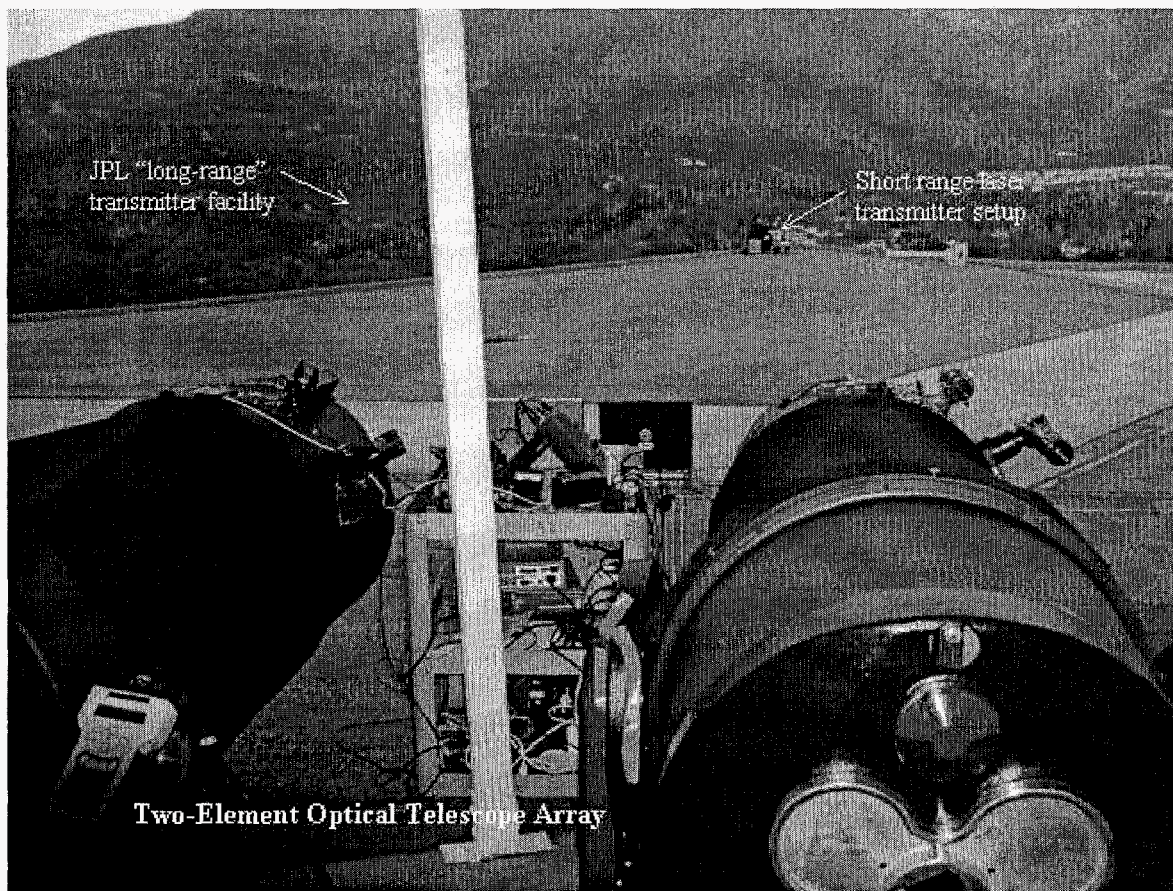


Figure 6. Experimental setup for reception of PPM modulated pulses directly from laser transmitter

Theoretical performance curves, showing the behavior of both uncoded 16-PPM, and Reed-Solomon coded 16-PPM symbols, is shown in Figures 7a and 7b. Bit error rates (BER) were computed as a function of the average number of signal photons, K_s , and also as a function of the photon information rate ρ . The additional performance improvements through the use of coding are also illustrated: with (15,7) Reed-Solomon coding applied to the 16-PPM symbols (that is, codewords consisting of 15 PPM symbols, with 7 information-bearing symbols, representing a rate 7/15 code) it can be seen in Fig. 7a that a BER of approximately 10^{-6} can be obtained with an average of 6 signal photons per pulse, as opposed to only about 10^{-2} for the uncoded case. Equation (20) was used to compute the approximate error rates for Reed-Solomon coded signals. The corresponding improvement, expressed in terms of photon information rate in Fig. 7b,

shows that approximately 2/3 bits per photon can be achieved through the use of coding at a BER of 10^{-6} , as opposed to only about 1/3 for the uncoded case. It should be recalled that the signal space is not limited to 16 PPM, but much higher dimensional signals such as 64 PPM or even 256 PPM can be employed in practical systems, for which the coding gains are even higher, potentially leading to dramatic improvements in optical array receiver performance.

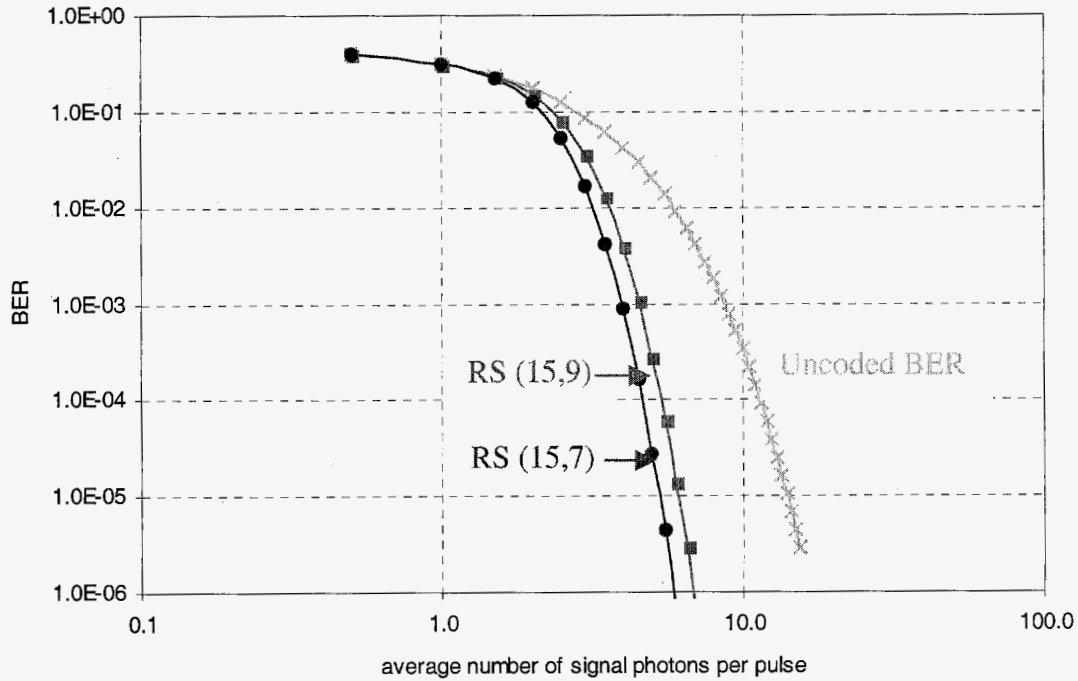


Figure 7a. BER vs Ks: theoretical uncoded and RS coded performance, with experimental points

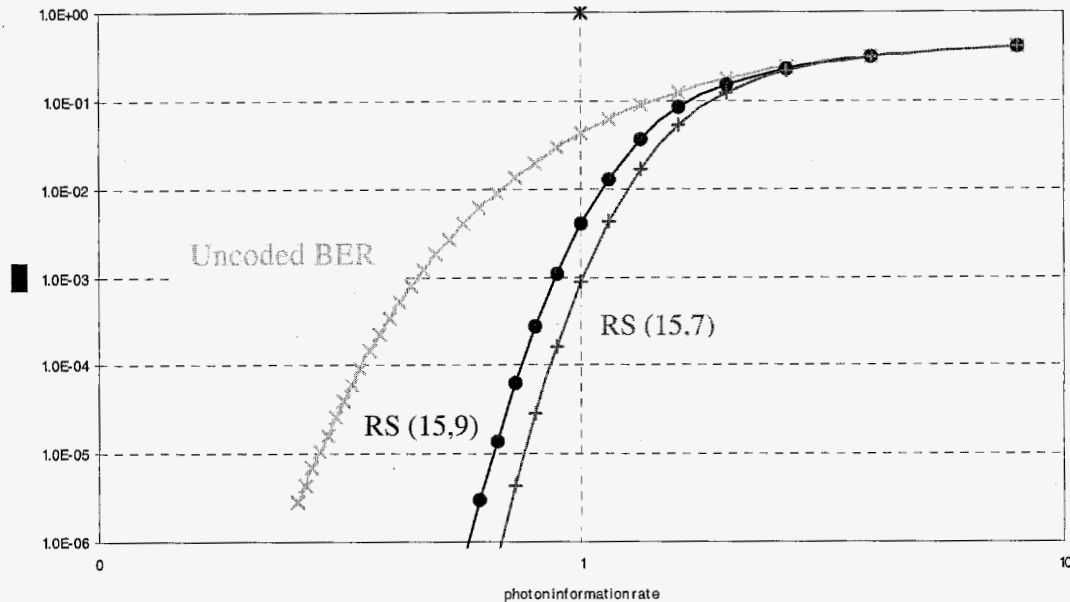


Figure 7b. Photon information rate vs Ks: theoretical uncoded and RS coded performance, with experimental points

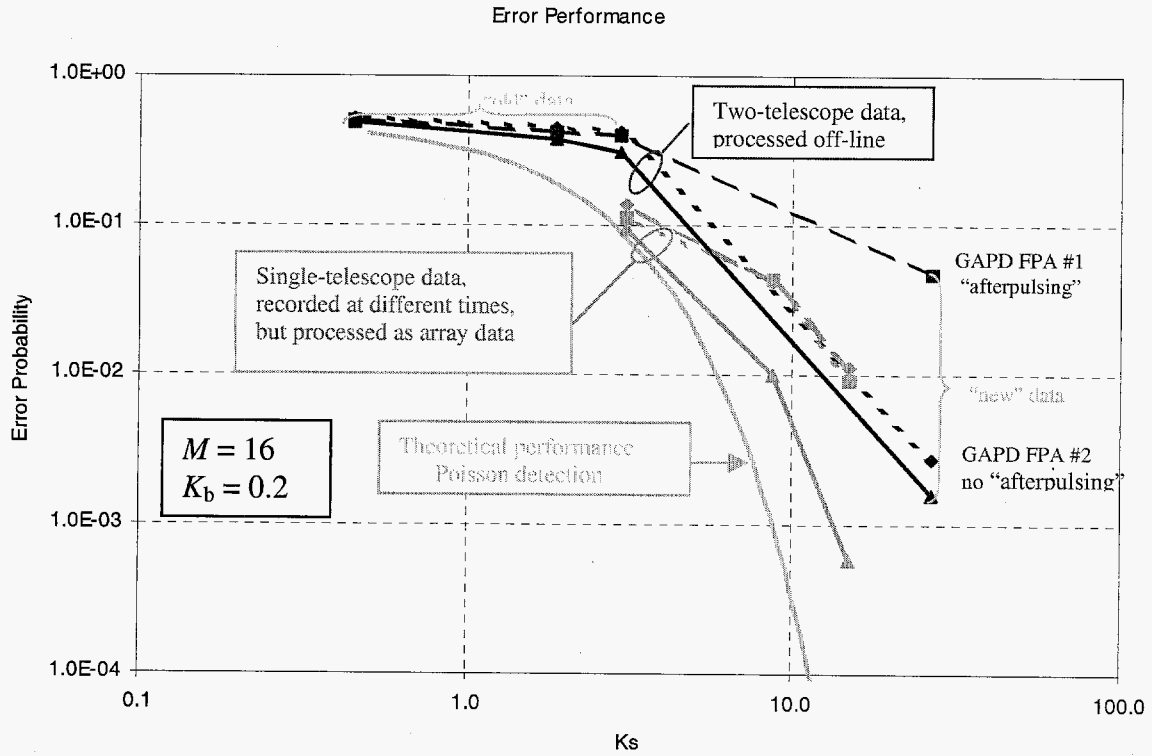


Figure 8a. Optical array receiver performance with experimental data: BER vs K_s .

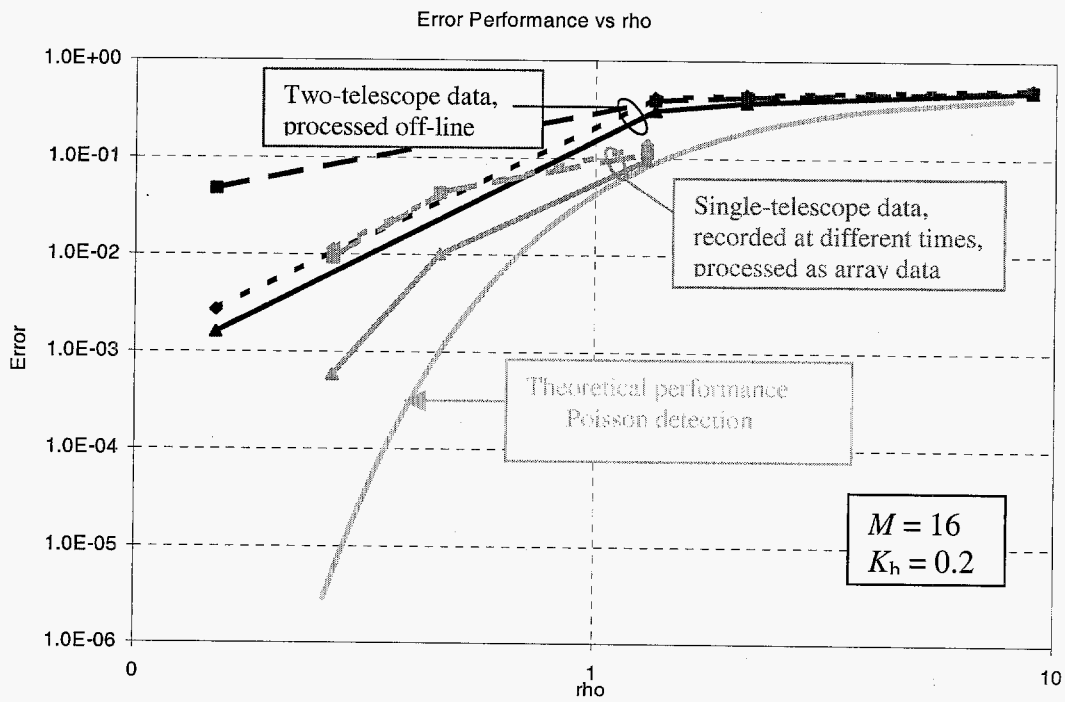


Figure 8b. Optical array receiver performance with experimental data: BER vs ρ .

Experimental data with the new setup was obtained in December, 2004. Data sets were again collected with both telescopes using neutral density filters at several drive voltages, resulting in a range of received signal intensities from the highest possible photon count of 16 (per 1 microsecond laser pulse), to virtually no received signal photons. These data were used as inputs to the delay-compensation and combining algorithm, and subsequently used for estimating array receiver performance. The processed field data are shown in Fig 8a and 8b, both as a function of average signal photons per pulse, and information rate (the data obtained in September is also shown as “old data”). It was found that one of the GAPD array detector assemblies (the first prototype design, the second unit incorporated numerous improvements) experienced significant afterpulsing, likely due to temperatures falling below 50 degrees that evening: this data is shown as the points labeled “new data” in Fig. 11. Therefore, data sets from each telescope with closely matched signal rates, taken under the same conditions and nearly the same time, were selected for evaluation. The experimentally obtained sequential data taken with the “good” detector, processed as two-telescope data and combined, already falls near the theoretical “uncoded BER” curves: this is the performance we expect with the improved design of the new detector assembly (already procured) after it is installed in the second telescope. Note that very significant gains in terms of decoded error performance can be obtained with the array, as compared to the performance of the individual array elements, when the signals from each telescope are adaptively delay-compensated and combined before symbol detection and decoding. The use of coding will further improve array performance, as illustrated in Fig. 7, but this improvement remains to be confirmed experimentally.

V. CONCLUSIONS

The research described in this article emphasizes the experimental verification of optical arraying concepts using a two-telescope optical array receiver, designed specifically for the reception of pulsed laser signals. The analysis, simulation and experimental results of previous years has now been extended to a two-telescope experimental array configuration, which for the first time enabled testing of key arraying and communications concepts in a realistic field environment. The ability to collect and combine sampled data from two telescopes in the field enabled testing and verifying the operations of optical photon-counting detection using Geiger-mode APD detector arrays, generation of photon-counting detector output samples at high rates, the delay compensation and combining algorithm with realistic field data, and offline software detection of pulsed signals. These functions have now been tested in the field and it has been shown that significant performance gains can be obtained using an array, based on physical measurements carried out in the field. While encouraging, these results remain to be extended to randomly modulated PPM symbols instead of periodic laser signals, and to real-time high data-rate operation in a relevant field environment, before a credible claim of a realistic Optical Array Receiver demonstration can be justified.

VI. REFERENCES

1. V. Vilnrotter, C.-W. Lau, M. Srinivasan, R. Mukai and K. Andrews, "Optical Array Receiver for Communication through Atmospheric Turbulence," accepted for publication in IEEE Transactions on Lightwave Technology.
2. V. Vilnrotter, C.-W. Lau, K. Andrews, M. Srinivasan, "Conceptual Design of an Optical Array Receiver, with Initial Experimental Results," IPN Progress Report 42-157, May 15, 2004.
3. V. Vilnrotter, C.-W. Lau, M. Srinivasan, R. Mukai, and K. Andrews, "An Optical Array Receiver for Deep-Space Communication through Atmospheric Turbulence," IPN Progress Report 42-154, August 15, 2003.
4. R. Gagliardi and S. Karp, *Optical Communications*, J. Wiley and Sons, New York, 1976.
5. M. Simon and V. Vilnrotter, "Performance Analysis and Tradeoffs for Dual-Pulse PPM on Optical Channels With Direct Detection," IEEE Transactions on Communications, vol. 52, no. 11, November 2004.
6. V. Vilnrotter and M. Srinivasan, "Adaptive Detector Arrays for Optical Communications Receivers," IEEE Transactions on Communications, Vol. 50, No. 7, July 2002.
7. R. J. McEliece and L. R. Welch, "Coding for Optical Channels With Photon-Counting," DSN Progress Report 42-52, May and June, 1979.
8. R. Sklar, *Digital Communications*, Prentice Hall, New Jersey, 1988.
9. G. Prati and R. Gagliardi, "Block Encoding and Decoding for the Optical PPM Channel," IEEE Transactions on Information Theory, Vol. IT-28, no. 1, January 1982.

CL# 04-3777
Kathy

OPTICAL ARRAY RECEIVER CONCEPT DEMONSTRATION

2004 Annual Report

JPL Task # R.04.023.029

*Drawings
cleared*

Victor Vilmrotter, Communications Systems and Research Section, (331)
Chi-Wung Lau, Meera Srinivasan, Kenneth Andrews, Norman Lay (Section 331)

A. OBJECTIVES

The objective of this research effort is to demonstrate a robust, scalable, and cost-effective ground-based optical array receiver in a relevant field environment, enabling high data-rate optical communications from space through the application of telescope and photodetector array algorithms and techniques. The theoretical foundations of optical array reception through atmospheric turbulence has been developed and documented as part of last year's effort. This year, the goal is to extend the scope of the research to include a preliminary field demonstration of key optical array receiver concepts, through a combination of field data-acquisition and offline signal processing. Next year, a realistic optical array receiver will be demonstrated in a relevant environment, with high-rate pulse-position modulated (PPM) optical signals processed and detected in real-time.

B. STRATEGIC FOCUS AREA

This work was performed in the Deep space communication / navigation Strategic Focus Area.

C. RELEVANCE TO STRATEGIC FOCUS AREA

A stated objective of future deep-space missions is to dramatically increase the useful data-rate, thus achieving greater science data return for each mission. This goal can be accomplished effectively through the use of optical rather than RF wavelengths. Due to cost and complexity considerations, the most practical approach at optical wavelengths is to employ a ground-based receiver, designed to mitigate the effects of atmospheric turbulence for best performance. A novel approach for ground-based optical communications is the concept of synthesizing a large optical aperture by means of an array of smaller telescopes, each containing a properly designed focal-plane array to reduce losses due to turbulence. Based on theoretical considerations and preliminary experimental results to date, the optical array receiver approach appears to be a viable and robust alternative to single large-aperture optical receivers.

D. APPROACH AND RESULTS

This year's research effort focused on extending the theoretical investigations carried out last year by constructing a two-telescope optical array receiver, capable of collecting and processing pulsed laser data in the field. This effort required the development of a detailed system design

that identified the signal processing functions, along with development of key components; development of signal processing algorithms to compensate for delay-variations of the received laser pulses between telescopes due to geometrical, instrumental and atmospheric effects; collection of pulsed laser data in the field; and demonstration of array combining gain by offline processing of the collected field data. This initial demonstration effort will lead directly to a more realistic optical communications demonstration in FY'05, where wideband pulse-position modulated (PPM) laser signals will be transmitted towards the two-telescope array, detected at each telescope via photon-counting detectors, combined in real-time to optimize receiver performance, and the resulting performance evaluated to demonstrate enhanced communications and establish practically achievable array gains.

After procurement and initial testing of a 25" computer-driven telescope in FY'03, a second 25" telescope was procured from the same manufacturer (JMI, Inc., of Colorado) in FY'04. A typical experimental setup on the JPL mesa antenna test range is shown in Fig. 1, where both telescopes can be seen pointing towards a retro-reflector assembly some 210 feet away. The retro-reflector assembly consists of a 65 mm diameter corner-cube reflector (from Edmund Scientific Co.) with a long focal-length lens in front, operating in a double-pass configuration: this optical arrangement expands the weak retro-reflected laser beam sufficiently to span the distance between the two telescopes. The laser transmitter assembly is located on the table between the two telescopes in Figure 1, and consists of a 5 milliwatt maximum power, 635 nm laser mounted in a fine-pointing bracket, and a pulse generator configured for 1 microsecond pulses repeating at 16 microsecond intervals. The laser is effectively gated "on" by the 1 microsecond pulses, and "off" for the following 15 microseconds, simulating a simple repetitive 16-PPM symbol suitable for test purposes.

The received optical energy is focused in each telescope, where it is first directed to a real-time CCD camera manufactured by SBIG, Inc., to extract position and intensity information prior to data-acquisition. The position information is used to fine-point the telescopes towards the retro-reflected beam. Following spatial acquisition, the CCD camera in each telescope is replaced by a high sensitivity geiger-mode avalanche photodiode (GAPD) detector array assembly custom-built by aPeak, Inc., shown in Figure 2a. These GAPD detector arrays consist of 4×4 detector elements, where each detector is capable of counting individual detected photons and generating a large (nominally 3 volt) pulse of 50 nanosecond duration in response to a photon detection event, as shown in Figure 2b. During field experiments, numerous signal photons were detected within each pulse-interval, delayed with respect to the electrical pulse due to the lagging response of the laser and drive electronics plus the round-trip light-time of approximately 420 nanoseconds, as illustrated in Figure 2c. A few background and "dark-count" photons can also be seen, occurring randomly.

The streams of electrical pulses generated by each detector array are captured by high-speed logic analyzer assemblies manufactured by GoLogic, Inc., and stored as samples of 8 nanosecond binary data, where each "1" represents a detector output voltage that exceeds a preset threshold (nominally 1.5 volts), while each zero represents lack of an output pulse. Therefore, a nominally 50 nanosecond electrical pulse is typically represented as a sequence of 6 to 7 binary ones, where each sample is 8 nanoseconds in duration. Each logic analyzer captures 4 million samples from every detector of the array, representing approximately 32 milliseconds of

data. The two logic analyzers have been configured to operate synchronously, enabling simultaneous data-acquisition from both telescopes. However, for efficient data-gathering in the field, it was necessary to use a separate computer for each logic analyzer to record the data. The synchronous logic analyzer assemblies, together with the notebook computers used for control and data-storage in the field, are shown in Figure 3.

After each field experiment the data was processed offline using custom algorithms, and the results analyzed to help improve the quality of the data-set during the next experiment. First, the binary outputs from the sixteen channels of each GAPD detector array are summed together. Since the detector output pulses tend to be approximately 50 nanoseconds in duration, the sampled electrical output pulses occur as runs of 6 or 7 “ones”, and it is the transitions from zero to one that are summed to obtain the photon counts. The current processing algorithms do not allow for optimal or near-optimal weighting of the individual detector output channels to account for the effects of particularly noisy detector elements or atmospheric turbulence: in this preliminary version, only the summed output of the entire focal-plane detector array is used. However, the added capability of optimal channel weighting will be incorporated in the next generation of signal processing algorithms.

The summed channel signals are converted to samples and a new data-file created, which serves as input to the adaptive delay-compensation algorithm. This algorithm was developed specifically to work with PPM signals detected with photon-counting detectors, and is intended to compensate for slowly-varying delay drift to ensure that PPM pulses received from each telescope are properly aligned in time before combining. The adapted delays for the i^{th} telescope (here i is either one or two, since there are only two telescopes) are formed according to an algorithm that resembles the well-known least mean square (LMS) and “constant modulus algorithm” (CMA) often employed to “phase up” conventional radio frequency arrays [1], except that here the delay adaptation is based entirely on the observed photon-counts. Denoting the PPM slot number by n and the delay variable by τ , the delay update algorithm for the i^{th} telescope is of the form:

$$\tau_i(n+1) = \tau_i(n) - \mu \left(\sum_{j \in \text{slot}} y_j(n) - y_0 \right)^2 \left[\sum_{j \in \text{slot} / 2}^{slot \text{ end}} s_{ji}(n) y_j(n) - \sum_{j \in \text{slot start}}^{slot / 2} s_{ji}(n) y_j(n) \right]$$

Cost function
Error signal

where j is the index of the sample within the n^{th} slot, $s_{ji}(n)$ are the summed photon-counts from the i^{th} telescope over the j^{th} sample of the n^{th} slot, $y_j(n)$ is the summed photon-count output of all telescopes over the j^{th} sample of the n^{th} slot, y_0 is the desired combined average photon-count of perfectly combined PPM sequences (usually determined from predicted or measured received signal power levels), and μ is the stepsize that controls the rate of the algorithm’s convergence and the degree of smoothing. The error signal is seen to be the difference of correlations of the received photon-count samples and the combined photon-count samples from the first and second halves of each slot. When the cost function approaches zero, the algorithm stops updating and continues to supply time-aligned combined samples to the receiver for further processing. An example of the array output resulting from processing two-telescope array field data, and of the behavior of the cost function as the delay differences were reduced by the

algorithm, is shown in Figure 4. Note that the cost function rapidly approaches zero, indicating that the two sample-streams have been effectively aligned after only a few PPM symbols have been processed.

Following delay compensation and combining, the software receiver forms sufficient statistics from the received combined samples, which in this case reduce to sums of sample-counts over each PPM slot. The optimum detection algorithm compares the slot-count over each PPM symbol and selects the symbol corresponding to the greatest slot-count [2, 3]. Since in our field experiments the signal pulse always occurred in the first slot, performance can be determined by comparing the symbol-decision made by the receiver with the known pulse location. This processing and error-estimation was carried out on data-sets taken in September, 2004. After initial telescope alignment and approximate signal-energy equalization, data was taken with various neutral density filters placed in front of the transmitter laser to attenuate the signal, as well as with an unattenuated laser. The results of processing this initial data set are shown in Figures 5a and 5b, where the symbol error rate (SER) performance of the array, together with the SER of each individual telescope, is shown both as a function of transmitter attenuation (filter density ND) and average photon-count per PPM signal-slot, K_s . In these initial data-sets only a few attenuations were used: the received laser power was weak to begin with, therefore the SER in these data-sets was generally quite high, in the neighborhood of 0.5 to nearly 1. This range, however, represents a reasonable operating region for coded operation, where subsequent decoding of the detected PPM symbols can yield bit error probabilities in the neighborhood of 10^{-6} . Note that in all cases, array performance is significantly better than the performance of the individual telescopes taken separately. While quite encouraging, these results must be extended to randomly modulated PPM symbols instead of periodic laser signals, and to real-time high data-rate operation in a relevant field environment, before a credible claim of a realistic Optical Array Receiver demonstration can be justified.

E. SIGNIFICANCE OF RESULTS

Large aperture optical receivers are difficult to construct and maintain, require massive support structures and drive assemblies, and represent a single point of failure in an optical communications system. Once constructed, the collecting area of a single large telescope cannot easily be expanded to meet future demands for enhanced performance. An array of small telescopes, on the other hand, provides a robust, scalable, parallel receiver architecture that can easily be expanded to accommodate higher data-rates or greater distances. The results obtained thus far indicate that the array receiver concept represents a viable alternative to the conventional "single large-aperture" approach for ground reception of optical deep-space signals.

F. FINANCIAL STATUS

The total funding for this task was \$206,000 all of which has been expended.

G. PUBLICATIONS

- [1] V. Vilnrotter, C.-W. Lau, M. Srinivasan, R. Mukai and K. Andrews, "Optical Array Receiver for Communication through Atmospheric Turbulence," accepted for publication in IEEE Transactions on Lightwave Technology.
- [2] V. Vilnrotter, C.-W. Lau, K. Andrews, M. Srinivasan, "Two-Element Optical Array Receiver Development and Initial Experimental Results," to appear in IPN Progress Report 42-159, November 15, 2004.
- [3] V. Vilnrotter, C.-W. Lau, M. Srinivasan, R. Mukai, and K. Andrews, "An Optical Array Receiver for Deep-Space Communication through Atmospheric Turbulence," IPN Progress Report 42-154, August 15, 2003.
- [4] V. Vilnrotter, C.-W. Lau, M. Srinivasan, R. Mukai and K. Andrews, "Optical Array Receivers for Deep Space Communication," 10th ISCOPS Conference, Tokyo, Dec. 6-8, 2003.
- [5] V. Vilnrotter, C.-W. Lau, M. Srinivasan, "Optical array receiver for deep-space communications," SPIE Proceedings, San Jose, CA, January 27, 2004.
- [6] V. Vilnrotter, C.-W. Lau, K. Andrews, M. Srinivasan, "Conceptual Design of an Optical Array Receiver with Preliminary Experimental Results," IPN PR 42-156, Feb. 15, 2003.

H. REFERENCES

- [1] L. Godara, "Application of Antenna Arrays to Mobile Communications," Proceedings of the IEEE, vol. 85, No. 8, August 1997.
- [2] R. Gagliardi and S. Karp, *Optical Communications*, J. Wiley and Sons, New York, 1976.
- [3] V. Vilnrotter and M. Srinivasan, "Adaptive Detector Arrays for Optical Communications," IEEE Transactions on Communications, Vol. 50, No. 7, July 2002.

I. FIGURES



Figure 1. Field configuration of two-element Optical Array Receiver, set up and aligned for data-gathering experiments over a horizontal path, on the JPL mesa antenna test range.

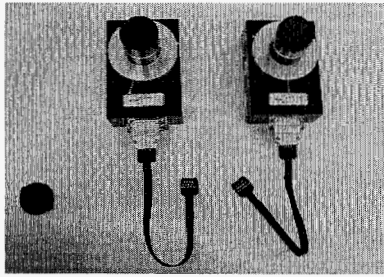


Figure 2a. Photon-counting focal-plane GAPD detector arrays (aPeak, Inc.)

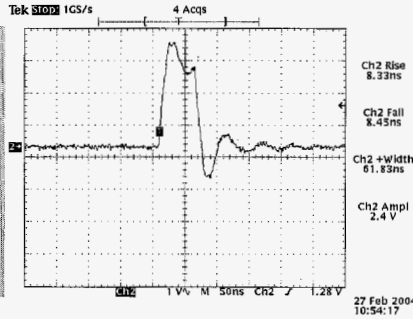


Figure 2b. Electrical response of GAPD array detector to a single photon (lab data)

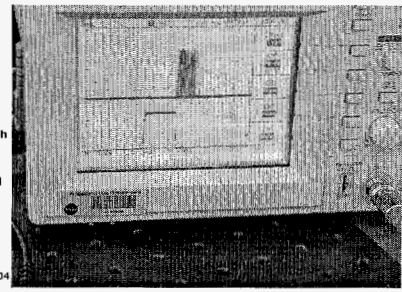


Figure 2c. Electrical response of GAPD array to a stream of photons (pulsed laser, field data)

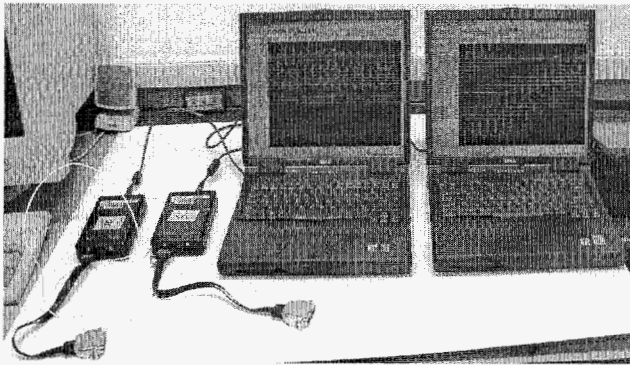


Figure 3. Logic analyzers manufactured by GoLogic, Inc., configured for synchronous operation, and notebook computers used for control and data-storage in the field.

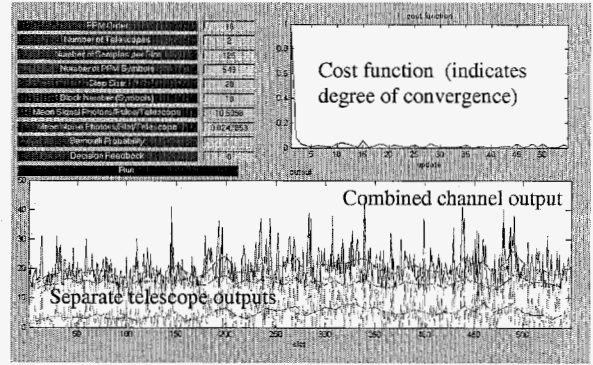


Figure 4. Example illustrating the output of delay compensation and combining algorithm

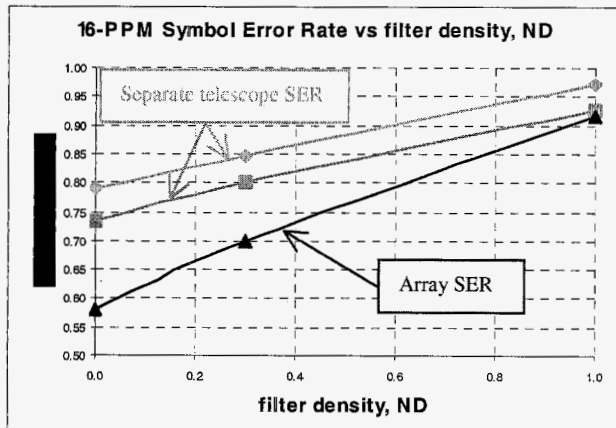


Figure 5a. Symbol error probability of experimentally obtained 16-PPM data, as a function of filter density ND.

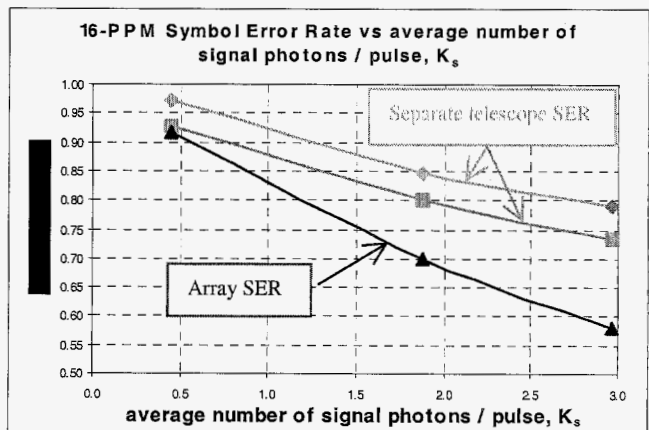


Figure 5b. Symbol error probability of experimentally obtained 16-PPM data, as a function of average signal-pulse photon count, K_s .